Published in final edited form as:
Blood. 2013 July 4; 122(1): 44–54. doi:10.1182/blood-2012-12-472845.

Parp-2 is required to maintain hematopoiesis following sublethal γ-irradiation in mice

Jordi Farrés[1], **Juan Martín-Caballero**[2], **Carlos Martínez**[3], **Juan J. Lozano**[3], **Laura Llacuna**[1], **Coral Ampurdanés**[1], **Cristina Ruiz-Herguido**[1], **Françoise Dantzer**[4], **Valérie Schreiber**[4], **Andreas Villunger**[5], **Anna Bigas**[1], and **José Yélamos**[1,3,6]

[1]Cancer Research Program, Hospital del Mar Medical Research Institute, Barcelona, Spain

[2]Barcelona Biomedical Research Park, Barcelona, Spain

[3]Centro de Investigación Biomédica en Red de Enfermedades Hepáticas y Digestivas, Barcelona, Spain

[4]Biotechnology and Cell Signaling, UMR7242-CNRS, Laboratory of Excellence Medalis, Ecole Supérieure de Biotechnologie de Strasbourg, Illkirch, France

[5]Division of Developmental Immunology, Biocenter, Innsbruck Medical University, Innsbruck, Austria

[6]Department of Immunology, Hospital del Mar, Barcelona, Spain

Abstract

Hematopoietic stem cells self-renew for life to guarantee the continuous supply of all blood cell lineages. Here we show that Poly(ADP-ribose) polymerase-2 (Parp-2) plays an essential role in hematopoietic stem/progenitor cells (HSPC) survival under steady-state conditions and in response to stress. Increased levels of cell death were observed in HSPC from untreated Parp-$2^{-/-}$ mice, but this deficit was compensated by increased rates of self-renewal, associated with impaired reconstitution of hematopoiesis upon serial bone marrow transplantation. Cell death after γ-irradiation correlated with an impaired capacity to repair DNA damage in the absence of Parp-2. Upon exposure to sublethal doses of γ-irradiation, Parp-$2^{-/-}$ mice exhibited bone marrow failure that correlated with reduced long-term repopulation potential of irradiated Parp-$2^{-/-}$ HSPC under competitive conditions. In line with a protective role of Parp-2 against irradiation-induced apoptosis, loss of p53 or the pro-apoptotic BH3-only protein Puma restored survival of irradiated Parp-$2^{-/-}$ mice, whereas loss of Noxa had no such effect. Our results show that Parp-2 plays essential roles in the surveillance of genome integrity of HSPC by orchestrating DNA repair and

Correspondence: José Yélamos, Department of Immunology, Hospital del Mar Medical Research Institute, Barcelona Biomedical Research Park, C/Dr Aiguader, 88, 08003, Barcelona, Spain; jyelamos@imim.es.
The online version of this article contains a data supplement.

Authorship
Contribution: J.F. carried out most of the experiments presented in the paper; J.M.-C. carried out BM transplant experiments; C.M. carried out pathology of BM sections and some microscopy experiments; J.J.L. performed gene expression arrays analysis; L.L. and C.R.-H. performed CFU experiments; C.A. provided technical assistance; J.M.-C., F.D., V.S., A.B., and A.V. designed experiments, provided reagents, and edited the paper; J.Y. planned and designed experiments, performed experiments and wrote the paper; and all authors discussed the results and commented on the manuscript.

Conflict-of-interest disclosure: The authors declare no competing financial interests.

Europe PMC Funders Author Manuscripts

restraining p53-induced and Puma-mediated apoptosis. The data may affect the design of drugs targeting Parp proteins and the improvement of radiotherapy-based therapeutic strategies.

Introduction

Poly(ADP-ribose) polymerase-2 (Parp-2) belongs to a family of enzymes that catalyze the transfer of ADP-ribose polymers to acceptor proteins. Among Parp family members, Parp-1, Parp-2, and Parp-3 catalytic activity has been shown to be stimulated by DNA breaks.1,2 Poly(ADP-ribosyl)ation, in response to DNA damage, coordinates chromatin decondensation around lesion sites, orchestrating the recruitment of repair proteins. Accordingly, these Parp proteins play a dual role in the DNA damage response, as damage sensors and signal transducers to downstream effectors through their physical association with or by the poly(ADP-ribosyl)ation of partner proteins.2,3 Parp-1 and Parp-2 possess overlapping functions as indicated by the early lethality of the double mutant embryos.4 Biochemical and structural studies increasingly predict that Parp-2 has particular targets and/or interacts with specific protein partners,5–7 suggesting functions independent of Parp-1 that only start to emerge. Parp-2 has been shown to be required for spermatogenesis,8 suppression of activation-induced deaminase–induced IgH/c-myc translocation,9 adipocyte differentiation,10 regulating SIRT1 expression to control body energy expenditure,11 and T-cell development and genomic stability in thymocytes accelerating spontaneous tumor development in Parp-2/p53-double-null mice.12,13

Mice lacking critical components of the DNA damage response machinery have been shown to display severe hematopoietic phenotypes,14–17 demonstrating that an appropriate DNA damage response is essential for the maintenance of normal hematopoiesis.18,19 The hematopoietic system is maintained by small numbers of hematopoietic stem cells (HSC) within the bone marrow (BM) that self-renew for life and give rise to a series of committed progenitors and all mature blood cells.20 Multiple pathways that regulate cell-cycle checkpoints, DNA repair, and apoptosis must be integrated delicately in HSPCs to regulate quiescence, self-renewal, and differentiation to guarantee maintenance of hematopoietic homeostasis throughout life.21–23 For example, previous studies have shown that ionizing radiation differentially affects subsets of BM hematopoietic cells, with HSC being more radio-resistant. This phenomenon has been ascribed to the engagement of the nonhomologous end-joining (NHEJ) pathway for DNA repair in HSCs to secure their survival, whereas their downstream progeny are poised to undergo apoptosis.19 Impairment of these fidelity control pathways can lead to genomic instability, hematopoietic malignancies, and BM failure.24,25 Indeed, exposure to a threshold level of genotoxic agents such as ionizing-radiation or DNA-damaging chemotherapeutics causes the loss of HSPC, leading to myeloablation-associated side effects in patients. Hence, understanding the mechanisms by which HSPC respond to DNA damage is pivotal for improved clinical management of treatment-associated side effects in transplantation settings or during the course of antineoplastic radio—or chemotherapy.

Here, we report on the critical role of Parp-2, but not Parp-1, in preventing BM failure and premature death of mice exposed to sublethal doses of irradiation. The premature lethality

Europe PMC Funders Author Manuscripts

observed in Parp-2$^{-/-}$ mice was associated with deficits in the DNA-damage response and increased HSPC apoptosis, rescued by p53 or Puma deficiency. Our results provide a novel role for Parp-2 as a mediator of HSPC homeostasis that may affect the improvement of radiotherapy-based therapeutic strategies.

Methods

Mice, radiation, and BM transplantation

Parp-1$^{-/-}$, Parp-2$^{-/-}$, Noxa$^{-/-}$, and Puma$^{-/-}$ mice have been described previously.4,26,27 p53$^{-/-}$ mice were obtained from Jackson Laboratories. Mice were of C57BL/6J background. Parp-2$^{-/-}$ mice were bred with p53$^{-/-}$ or Noxa$^{-/-}$ or Puma$^{-/-}$ mice to generate heterozygous mice, which were then bred to generate all genotypes. Genotyping was performed by polymerase chain reaction (PCR).4,12,27,28 CD45.1 mice (B6.SJL-ptprcPep3) were from the European Molecular Biology Laboratory (Heidelberg, Germany). Mouse studies were approved by the PRBB Animal Care Committee. γ-Irradiation and BM transplantation details are indicated in supplementary Methods.

Whole-blood analysis and histology

Blood was analyzed using Abacus Junior Vet Haematology Blood Analyzer. Histology details are indicated in supplementary Methods.

Flow cytometry, cell sorting, and ROS analysis

Cells were stained with various antibodies and analyzed with a LSRII cytometer (BD Biosciences) using DIVA (BD Biosciences) and FlowJo (TreeStar) software. Fluorescence-activated cell sorting was performed in a FACS ArialISORP (BD Biosciences). Reactive oxygen species (ROS) levels were measured by suspending cells in phosphate-buffered saline containing 5 μM 5-(and-6)-carboxy-2′,7′- difluorodihydrofluorescein-diacetate. Details are available in supplementary Methods.

BrdU incorporation

Mice received a single intraperitoneal injection of BrdU (BD Biosciences; 1 mg/6 g mouse weight) and admixture of 1 mg/mL of BrdU to drinking water for 3 days. BM cells were surface-stained, fixed, permeabilized, and intracellularly stained using a BrdU Flow kit (BD Biosciences).

Colony formation assays

Hematopoietic progenitors in BM cells were evaluated by colony assays scored at day 7 using MethoCult M3434 methylcellulose semisolid medium (StemCell Technologies).

Immunofluorescence and comet assay

Immunofluorescence and alkaline comet assay on Lin$^-$(CD11b$^-$Gr1$^-$B220$^-$CD3$^-$Ter119$^-$)Sca-1$^+$c-kit$^+$ (LSK)- and myeloid progenitor (MP)–sorted cells was performed as indicated in supplementary Methods.

Gene expression

Total RNA isolation, quantitative reverse-transcriptase PCR (RT-PCR), and microarray were performed as indicated in supplementary Methods. Microarray data have been deposited into the Gene Expression Omnibus (GSE42022).

Statistical analysis

The log-rank test was used to determine the statistical significance of animal survival. All other statistical analyses used an unpaired Student *t* test. *P* values < .05 were considered significant.

Results

Parp-2–deficient mice show increased sensitivity to sublethal γ-irradiation dose caused by BM failure

Parp-$2^{-/-}$ and Parp-$1^{-/-}$ mice were shown to be very sensitive to high doses of whole-body ionizing radiation (8 Gy), probably because of acute radiation toxicity to the epithelium of the small intestine.4 In contrast, low-dose radiosensitization was not apparent in Parp-$1^{-/-}$ cells, likely suggesting a compensating activity by Parp-2.29 However, the sensitivity of Parp-$2^{-/-}$ mice to sublethal doses of irradiation remained unexplored. To address this, Parp-$2^{-/-}$ and WT littermate mice were exposed to a sublethal dose of 5 Gy of total-body γ-irradiation (TBI). WT mice survived beyond 35 days, whereas all Parp-$2^{-/-}$ mice died at a median of 18 days. Interestingly, 7 of 8 Parp-1–deficient mice survived (Figure 1A), indicating a differential or tissue type–specific contribution of Parp-1 and Parp-2 in the response to low-dose γ-irradiation. Similarly, specific sensitivity of Parp-$2^{-/-}$, but not Parp-$1^{-/-}$, mice was observed in a cumulative low-dose irradiation protocol of 4 weekly doses of 1.75 Gy (supplemental Figure 1A). The death of Parp-$2^{-/-}$ mice after exposure to 5 Gy TBI suggested either BM failure or cumulative systemic effects of radiation. We addressed this issue by transplanting WT BM cells into Parp-$2^{-/-}$ recipient mice that had received 5 Gy. The WT BM cells rescued the irradiated Parp-$2^{-/-}$ mice from death (Figure 1A), indicative of BM failure as the cause of death in Parp-$2^{-/-}$ mice. Notably, histopathology did not reveal any signs of infection (supplemental Figure 2).

To test whether WT BM cells can radioprotect Parp-2–deficient mice in a cell-autonomous manner, Parp-$2^{-/-}$ mice were lethally irradiated (9.5 Gy) and transplanted with BM cells from either WT or Parp-$2^{-/-}$ mice. Six weeks after reconstitution, recipients received TBI (5 Gy). The majority of Parp-$2^{-/-}$ mice reconstituted with WT BM cells lived more than 35 days after the second dose of γ-irradiation. In contrast, all Parp-$2^{-/-}$ mice reconstituted with Parp-$2^{-/-}$ BM cells died within 20 days after the second irradiation (Figure 1B). To test whether Parp-$2^{-/-}$ BM cells could radioprotect mice within a WT microenvironment, we reconstituted lethally irradiated WT mice with WT or Parp-$2^{-/-}$ BM cells. Six weeks after transplantation, the mice received 5 Gy of TBI. Only the mice reconstituted with Parp-$2^{-/-}$ BM cells became radiosensitive (Figure 1B). These results implicate accentuated radiation-induced damage to HSPC in the death of Parp-$2^{-/-}$ mice after exposure to a sublethal dose of TBI in a hematopoietic cell-autonomous manner.

Repopulation of hematopoietic cells is impaired in irradiated Parp-2–deficient mice

Parp-$2^{-/-}$ mice show slightly lower RBC but similar WBC counts at baseline. Consistent with previous studies,30 we observed a striking decrease in WBC counts and a slower decrease in RBC in WT mice at days 4, 6, and 12 post irradiation. However, Parp-$2^{-/-}$ mice exhibited more severe decreases in RBC counts, whereas the decrease in WBCs was slightly more severe compared with WT mice only at day 12 (Figure 1C). BM cellularity in Parp-$2^{-/-}$ and WT mice was similar before irradiation and dropped significantly by day 4 post irradiation to similar levels. By day 6 after γ-irradiation, BM cells began to rebound and this recovery was less effective in Parp-$2^{-/-}$ mice compared with WT mice (Figure 1D). Histologic analysis revealed that by day 12 post irradiation, hematopoietic cell clusters had repopulated the BM of WT mice but not those of Parp-$2^{-/-}$ mice (Figure 1E).

Analysis of the HSC-containing LSK population showed that the percentages and total numbers of LSK cells in untreated WT and Parp-$2^{-/-}$ mice were similar (Figure 2). Further analysis of the LSK compartment showed that the enriched long-term HSC population (LT-HSC;$Lin^{-}Sca\text{-}1^{+}c\text{-}kit^{+}CD135^{-}CD34^{-}$), the enriched short-term HSC population (ST-HSC; $Lin^{-}Sca\text{-}1^{+}c\text{-}kit^{+}CD135^{-}CD34^{+}$), and the multipotent progenitors (MPPs; $Lin^{-}Sca\text{-}1^{+}c\text{-}kit^{+}CD135^{+}CD34^{+}$) fractions were similar in WT and Parp-$2^{-/-}$ mice (Figure 2). Similarly, in the MP compartment, percentages and total numbers of common MPs (CMP; $Lin^{-}Sca\text{-}1^{-}c\text{-}kit^{+}CD34^{+}Fc\gamma R^{lo}$), myelomonocytic progenitors (GMP; $Lin^{-}Sca\text{-}1^{-}c\text{-}kit^{+}CD34^{+}Fc\gamma R^{hi}$), and megakaryocyte/erythroid progenitors (MEP;$Lin^{-}Sca\text{-}1^{-}c\text{-}kit^{+}CD34^{-}Fc\gamma R^{lo}$) were comparable in WT and Parp-2 mice under steady-state conditions (Figure 2).

By day 12 after TBI (5 Gy), Parp-$2^{-/-}$ mice retained fewer number of LSK cells than WT mice. Similarly, a reduction in the LT-HSC was observed in Parp-$2^{-/-}$ compared with WT mice, whereas ST-HSC and MPP fractions were similar in both genotypes (Figure 2C). Furthermore, a striking decrease in the number of all MP populations (CMP, GMP, and MEP) was observed in Parp-$2^{-/-}$ compared with WT mice (Figure 2C). These results suggest that Parp-$2^{-/-}$ HSPC exhibits increased sensitivity to irradiation, affecting normal restoration of hematopoiesis after sublethal irradiation.

Interestingly, when we tested the colony-formation capacity of basal WT or Parp-$2^{-/-}$ BM cells in methylcellulose, we observed that Parp-$2^{-/-}$ cells displayed a significantly decreased capacity to form colony-forming units (CFUs) compared with WT BM cells (Figure 2D). In response to 2 Gy, the colony-forming potential dropped significantly in Parp-$2^{-/-}$ and WT cells and the significant decrease in CFU from Parp-$2^{-/-}$ compared with WT persisted (Figure 2D).

Reduced regenerative capacity of Parp-2–deficient HSPC after expansion stress

The radiosensitivity of Parp-$2^{-/-}$ mice may reflect loss of committed hematopoietic progenitors but also a defect in the regenerative capacity of the HSC pool. To test this possibility, WT or Parp-$2^{-/-}$ mice ($CD45.2^{+}$) were irradiated with a dose of 5 Gy and transplanted with BM cells from WT (B6.SJL) mice expressing CD45.1. Analysis at 6 and 12 weeks after transplantation showed that only 6% of peripheral blood cells in the

transplanted Parp-2$^{-/-}$ mice originated from the recipients compared with ~30% of peripheral blood originated from the WT recipient control mice (Figure 3A). These data suggest a radiation-induced defect in Parp-2$^{-/-}$ HSC regenerative capacity compared with WT.

To further characterize the radiation-induced defect in Parp-2$^{-/-}$ HSC, we performed competitive repopulation assays. WT or Parp-2$^{-/-}$ BM cells were isolated after TBI (2 Gy or 5 Gy), mixed at a 19:1 ratio with nonirradiated WT (B6.SJL) competitor BM cells, and transplanted into lethally irradiated (9.5 Gy) B6xB6.SJL F1 recipient mice (CD45.1/2) (Figure 3B). In recipients receiving WT BM cells exposed to 5 Gy and nonirradiated competitor cells, ~4% of blood cells were derived from the irradiated WT donor HSCs at 12 weeks after transplantation. Identical analysis in the mice transplanted with 5 Gy–treated Parp-2$^{-/-}$ BM cells and nonirradiated WT competitor cells revealed that only ~0.6% of blood cells were derived from the irradiated Parp-2$^{-/-}$ HSCs, indicating a significantly poorer performance of HSC from Parp-2$^{-/-}$ compared with WT in this competitive situation (Figure 3C). As expected, we observed an increase in engraftment of 2 Gy irradiation–exposed HSC, but a significant defect of engraftment of Parp-2$^{-/-}$ HSCs persisted (Figure 3C). Of note, BM cells from nonirradiated WT and Parp-2$^{-/-}$ donor mice showed comparable ability to repopulate the peripheral blood (Figure 3C). However, Parp-2$^{-/-}$ BM cells showed impaired repopulation potential in secondary transplants (Figure 3D). These results indicate that Parp-2$^{-/-}$ HSC function is compromised after expansion stress such as the one caused by irradiation or BM serial transplantations.

Parp-2 regulates HSPC survival

Decreased numbers of HSPCs in Parp-2$^{-/-}$ mice after irradiation could reflect impaired proliferation, cell survival, or a combination of these. To evaluate the proliferation rate, mice received a single intraperitoneal injection of BrdU, and then we provided BrdU in the drinking water for 3 days. Analysis of LSK and MP cells on the fourth day showed statistically significant increased BrdU incorporation in Parp-2$^{-/-}$ compared with WT LSK cells and a trend toward an increase in Parp-2$^{-/-}$ MP cells, suggesting that Parp-2 deficiency does not limit proliferation of LSK or MP cells (Figure 4A-B). Next we assessed the cell-cycle status by Ki67 staining to detect cycling cells and 4′,6-diamidino-2-phenylindole to gauge the amount of DNA. Gating on the LSK- and MP-cell fractions revealed a decrease of cells in G0 in Parp-2$^{-/-}$ compared with WT cells, although statistically significant differences were not achieved (Figure 4C-D).

Interestingly, both Parp-2$^{-/-}$ LSK and MP cells displayed higher levels of intracellular ROS (Figure 4E-F), which have been linked to proliferation31 but may also cause higher rates of DNA-damage and possibly cell death. Hence, we used active caspase-3 staining to compare the levels of apoptosis in HSPCs from Parp-2$^{-/-}$ and wild-type mice. Parp-2$^{-/-}$ cells exhibited a significantly higher number of active caspase-3–positive cells than WT under homeostatic conditions. At 2 hours after 5 Gy of irradiation, active caspase-3-positive cells increased significantly in both Parp-2$^{-/-}$ and WT mice, and the significant increase in apoptotic cells in Parp-2$^{-/-}$ compared with WT persisted (Figure 4G-H). Similarly, the percentage of AnnexinV^{+} LSK and MP cells was also higher in Parp-2$^{-/-}$ than in WT mice

(supplemental Figure 3). These results suggest that restoration of hematopoiesis after sublethal irradiation requires Parp-2, most likely restraining the apoptotic response in HSPCs.

Loss of p53 or Puma, but not loss of Noxa, suppresses the radiosensitivity of Parp-2-deficient mice

To investigate the functional interaction of Parp-2 with the p53-mediated apoptotic pathway in HSPC, we generated mice lacking both genes and analyzed the effect of 5 Gy TBI. Parp-$2^{-/-}$p$53^{-/-}$ mice survived TBI beyond 35 days, indicating that inactivation of p53 rescued Parp-$2^{-/-}$mice from radiation-induced death (Figure 5A). To further explore whether Parp-2 deficiency engages a p53-dependent response, we determined p53 protein levels in LSK and MP cells. We observed an increase in p53 protein levels in Parp-$2^{-/-}$ compared with WT cells at basal and 2 hours post irradiation, suggesting an increased p53 response in the absence of Parp-2 (Figure 5B-C). Of note, p53 protein levels in Parp-$1^{-/-}$ LSK and MP cells were similar to those found in WT cells (supplemental Figure 4). Puma and Noxa play critical roles in p53-mediated apoptotic pathways.27 Accordingly, we examined whether Parp-2 deficiency affects the induction of either of these p53 target genes by quantitative RT-PCR. Baseline Puma mRNA levels were significantly higher in Parp-$2^{-/-}$ compared with wildtype LSK cells. A similar trend was noted in Parp-$2^{-/-}$ MP cells. At 2 hours after irradiation, Puma mRNA levels increased significantly in both Parp-$2^{-/-}$ and WT LSK cells, and a significant increase persisted in Parp-$2^{-/-}$ compared with WT irradiated LSK cells. Interestingly, mRNA levels of Puma were similar in Parp-$1^{-/-}$ and WT LSK and MP cells (Figure 5D). By contrast, baseline Noxa mRNA expression was lower in Parp-$2^{-/-}$ than in WT LSK cells, whereas similar expression was observed in MP cells. Upon irradiation, Noxa mRNA levels increased, but this effect was less pronounced in Parp-$2^{-/-}$ compared with WT LSK and persisted in MP cells. Noxa expression in Parp-$1^{-/-}$ LSK and MP cells followed the expression in Parp-$2^{-/-}$ cells (Figure 5D).

To test the physiological significance of our findings, we generated mice lacking Parp-2 and either Puma or Noxa genes. Puma deficiency rescued Parp-$2^{-/-}$ mice from 5 Gy TBI-induced death, whereas the loss of Noxa had no effect (Figure 5E). In agreement with our survival data, we observed that the reduced RBC, WBC, and BM cellularity in Parp-$2^{-/-}$ mice, noted at day 12 post irradiation, was completely restored in a Puma-deficient but not in a Noxa-deficient background (Figure 5F). Indeed, p53 and Puma expression were significantly increased in Parp-$2^{-/-}$ compared with WT erythroblasts (supplemental Figure 5).

Impaired DNA damage response in Parp-2–deficient HSPC

LSK and MP cells from nonirradiated mice of both genotypes displayed extremely low levels of γ-H2AX–positive cells, an indicator of double-strand breaks (DSBs),32 which was markedly induced after exposure to 5 Gy TBI. By 2 hours post irradiation of mice, the numbers of γ-H2AX–positive cells in Parp-$2^{-/-}$ LSK and MP cells was significantly higher than that noted in WT cells, suggesting an increased sensitivity to DNA damage (Figure 6A-B). These results were confirmed by immunostaining of γ-H2AX and immunofluorescence microscopy (supplemental Figure 6).

We next subjected LSK and MP cells to an alkaline comet assay to assess induction and repair of DNA breaks independently from their signaling and processing markers. We observed a significant increase of cells displaying comet shape in LSK cells from Parp-$2^{-/-}$ mice at basal and at one and two hours post TBI compared with wild-type LSK cells (Figure 6C-D). We also observed a slight increase in MP cells from Parp-$2^{-/-}$ compared with WT mice before and 2 hours post irradiation.

To test whether Parp-2 deficiency impaired DSB repair, we quantified Rad51-containing ionizing radiation-induced foci and 53BP1-containing ionizing radiation-induced foci as markers of homologous recombination (HR) and NHEJ pathways, respectively. We observed a similar percentage of Parp-$2^{-/-}$ and WT cells with Rad51-positive and 53BP1-positive foci (supplemental Figure 7A-B). We also analyzed the expression of HR and NHEJ components in LSK and MP cells by quantitative RT-PCR. Basal levels of HR and NHEJ components were either similar or higher (Rpa.a1 and Xrcc2) in Parp-$2^{-/-}$ compared with WT cells. Upon irradiation, similar or higher (Smc6 and Ku80) expression levels of these DNA repair components were found in Parp-$2^{-/-}$ compared with WT cells, except for Rad54 (supplemental Figure 7C). Altogether, our data suggest that Parp-2 deficiency probably leads to elevated single-strand breaks, which are rapidly converted to DSBs in the S phase instead of a decreased in DSB repair per se.

Gene-expression analyses of Parp-2–deficient HSPCs reveals changes in the DNA damage response pathways

To gain further insights into the effect of Parp-2 deficiency on HSPCs, we performed microarray on purified LSK and MP cells from Parp-$2^{-/-}$ and WT mice, both at 0 and 2.5 hours after TBI. Bioinformatics analyses showed that in the absence of Parp-2, more prevalent gene expression changes were detected in the LSK population rather than in the MP population (supplemental Figure 8). Clustering of all genes that changed between Parp-$2^{-/-}$ and wild-type cells is represented in Figure 7A.

Gene Set Enrichment Analysis (GSEA)33 showed enrichment for signatures of cell cycle, DNA replication, DNA repair, and apoptosis in PARP-$2^{-/-}$ compared with WT cells at the steady-state level (Figure 7B-C). Two and a half hours after TBI (5 Gy), a significant enrichment of different pathways such as apoptosis, cell-cycle checkpoints, and base excision repair was also observed in Parp-$2^{-/-}$ cells (Figure 7B-C). In summary, bioinformatics analyses showed a strong enrichment for genes involved in the DNA damage response in Parp-$2^{-/-}$ compared with WT HSPCs, thus supporting the functional effect of Parp-2 in orchestrating recovery of LSK and MP cells after DNA damage.

Discussion

Here, we have shown that genetic inactivation of Parp-2 in mice, but not of Parp-1, resulted in BM failure in response to sublethal γ-irradiation dose, providing the first evidence for an important and nonredundant role of Parp-2 to properly maintain hematopoietic homeostasis. Radiosensitivity in the hematopoietic compartment is determined by the severity of irradiation-induced apoptosis in hematopoietic cells during the acute phase, and by the ability of HSPCs to replace the damaged cells during the recovery phase. Our data indicated

an increased sensitivity of γ-irradiated Parp-2–deficient HSPCs to apoptosis, mainly myeloerythroid-restricted progenitors, which have the predominant role in short-term radio-protection.34 Indeed, our microarray data show a significant enrichment for genes belonging to apoptosis pathway in Parp-$2^{-/-}$ compared with WT MP cells. Moreover, the irradiation-induced BM failure in Parp-$2^{-/-}$ mice was abolished in a p53-deficient background as well as in a Puma-deficient background, whereas loss of Noxa had no effect. Our data agree with previous reports showing that p53, through Puma expression, plays a critical role in the apoptotic response to DNA damage in hematopoietic cells, whereas Noxa is largely dispensable.27,35–37 Interestingly, our competitive BM transplant assays show that BM cells from irradiated Parp-$2^{-/-}$ mice also exhibited reduced repopulating efficiency than BM cells from irradiated WT mice, revealing a high sensitivity to low doses of irradiation of Parp-2–deficient HSCs, leading to impaired repopulating potential. Altogether, our data suggest a role of Parp-2 in the resistance of HSPC to p53-dependent apoptosis induced by γ-radiation.

The increased apoptosis observed in HSPC from irradiated Parp-$2^{-/-}$ mice was accompanied by an increase in DNA damage, suggesting a specific role of Parp-2 in the DNA damage response in HSPCs. These data are in agreement with a report showing that BM cells taken from 2 Gy–irradiated mice presented an increase of chromatid breaks in the Parp-$2^{-/-}$ background, suggesting a DNA repair deficiency of radiation-induced damage, mainly in the S phase and during G2.4 Interestingly, hypersensitivity to low-dose radiation has been proposed to be a consequence of ineffective cell-cycle arrest of radiation-damaged G2-phase cells.38 Moreover, chromatid breaks occurred more frequently in centromeric regions in Parp-$2^{-/-}$ cells than in WT cells, thus providing evidence for a possible role for Parp-2 in the maintenance of centromeric heterochromatin integrity,39 and a role in accurate chromosome segregation.8 Interestingly, our microarray data reveal significant enrichment of a cell-cycle checkpoints pathway in irradiated Parp-$2^{-/-}$ LSK cells compared with WT, suggesting an effect of Parp-2 in LSK cycling in response to irradiation. However, we cannot rule out that changes in expression on cell cycle genes in Parp-$2^{-/-}$ LSK cells may be caused by the need to replenish the periphery and not directly caused by the loss of Parp-2.

Despite the increased apoptosis level observed in Parp-$2^{-/-}$ HSPCs at basal conditions, the total number of cells was similar in both genotypes. These results are consistent with a compensatory proliferation by previously quiescent HSPCs to replace the increased level of cell death. Indeed, under steady-state conditions, we have observed a significantly increased percentage of BrdU-positive cells in Parp-$2^{-/-}$ LSK cells that was accompanied by a slight decrease in the percentages of Parp-$2^{-/-}$ LSK in G0/quiescence. Interestingly, Parp-$2^{-/-}$ BM cells show impaired repopulation potential in secondary transplants, suggesting the exhaustion of HSCs. An enrichment of cell cycle, DNA replication, and DNA repair functional categories in the transcriptome of Parp-$2^{-/-}$ LSK cells compared with WT LSK cells was also observed. These data suggest the activation of the apoptotic pathway in Parp-$2^{-/-}$ HSPCs in response to an increased genomic instability that may be associated with replication stress. The accelerated proliferation observed in Parp-$2^{-/-}$ cells may lead to DNA damage through overexposure to oxidative stress mediated by ROS production during cell cycle,40 which is also an important regulator of HSC mobilization.22,41 Accordingly, we have also observed increased ROS levels in Parp-$2^{-/-}$ HSPCs compared with WT cells.

Our results are consistent with a model (supplemental Figure 9) whereby under low levels of DNA damage caused by intrinsic ROS levels, inefficient DNA damage response in the absence of Parp-2 leads to cumulative DNA damage and activation of p53-dependent apoptotic pathways. However, this increased cell death may be compensated by an increase in HSC proliferation, which may actually also be cause or consequence of increased levels of ROS.31 Our results suggest that this strategy is sufficient to replenish the hematopoietic compartment in basal conditions in Parp-$2^{-/-}$ mice. Conversely, after exposing mice to sublethal doses of γ-irradiation, high levels of DNA damage and massive cell death take place. In the absence of Parp-2, inefficient DNA damage response increases apoptosis of hematopoietic cells. In addition, HSCs that have been forced to proliferate more readily in the absence of Parp-2 appear to become even more vulnerable than their more quiescent HSC counterparts in WT mice, in agreement with published results.19 This increased vulnerability results in BM failure and premature death of Parp-$2^{-/-}$ mice.

Currently, there is considerable excitement about the prospect of anticancer compounds that act through the targeting of Parp proteins. Our observation is that Parp-2–mediated radioresistance of HSPCs may also have implications in the design of drugs targeting Parp proteins. For instance, specifically targeting Parp-2 might be useful to increase the sensibility of cancer stem cells to radiation treatment.18,42 On the other hand, inhibitors targeting Parp-1 specifically may be less toxic and avoid BM failure. In summary, our results show that Parp-2 plays essential roles in the DNA damage response in HSPCs, both in homeostatic conditions and in response to irradiation stress.

Supplementary Material

Refer to Web version on PubMed Central for supplementary material.

Acknowledgments

The authors thank P. Moreno, M. Juan, and S. Capdevila for assistance with the mice; R. Gimeno and P. Aparicio for useful comments; O. Fornes for cell sorting and flow cytometry assistance; E. Puigdecanet and L. Nonell for microarrays support; S. Mojal for statistical analysis support; and A. Strasser for Puma- and Noxa- deficient mice.

This work was supported by the Spanish Ministerio de Economía y Competitividad (HA2008-0010, SAF2008-01572, SAF2011-26900), Generalitat de Catalunya (2009/SGR/524), Fundación Mutua Madrileña (J.Y.), Juan de la Cierva fellowship program (L.L.), and the Austrian Science Fund (FWF, Y212-B12, SFB021) (A.V.).

References

1. Boehler C, Gauthier LR, Mortusewicz O, et al. Poly(ADP-ribose) polymerase 3 (PARP3), a newcomer in cellular response to DNA damage and mitotic progression. Proc Natl Acad Sci USA. 2011; 108(7):2783–2788. [PubMed: 21270334]
2. Yélamos J, Schreiber V, Dantzer F. Toward specific functions of poly(ADP-ribose) polymerase-2. Trends Mol Med. 2008; 14(4):169–178. [PubMed: 18353725]
3. Gibson BA, Kraus WL. New insights into the molecular and cellular functions of poly(ADP-ribose) and PARPs. Nat Rev Mol Cell Biol. 2012; 13(7):411–424. [PubMed: 22713970]
4. Menissier, dM; Ricoul, M.; Tartier, L., et al. Functional interaction between PARP-1 and PARP-2 in chromosome stability and embryonic development in mouse. EMBO J. 2003; 22(9):2255–2263. [PubMed: 12727891]
5. Isabelle M, Moreel X, Gagné JP, et al. Investigation of PARP-1, PARP-2, and PARG interactomes by affinity-purification mass spectrometry. Proteome Sci. 2010; 8:22. [PubMed: 20388209]

6. Oliver AW, Amé JC, Roe SM, Good V, de Murcia G, Pearl LH. Crystal structure of the catalytic fragment of murine poly(ADP-ribose) polymerase-2. Nucleic Acids Res. 2004; 32(2):456–464. [PubMed: 14739238]
7. Troiani S, Lupi R, Perego R, et al. Identification of candidate substrates for poly(ADP-ribose) polymerase-2 (PARP2) in the absence of DNA damage using high-density protein microarrays. FEBS J. 2011; 278(19):3676–3687. [PubMed: 21812934]
8. Dantzer F, Mark M, Quenet D, et al. Poly(ADP-ribose) polymerase-2 contributes to the fidelity of male meiosis I and spermiogenesis. Proc Natl Acad Sci USA. 2006; 103(40):14854–14859. [PubMed: 17001008]
9. Robert I, Dantzer F, Reina-San-Martin B. Parp1 facilitates alternative NHEJ, whereas Parp2 suppresses IgH/c-myc translocations during immunoglobulin class switch recombination. J Exp Med. 2009; 206(5):1047–1056. [PubMed: 19364882]
10. Bai P, Houten SM, Huber A, et al. Poly(ADP-ribose) polymerase-2 [corrected] controls adipocyte differentiation and adipose tissue function through the regulation of the activity of the retinoid X receptor/peroxisome proliferator-activated receptor-gamma [corrected] heterodimer. J Biol Chem. 2007; 282(52):37738–37746. [PubMed: 17951580]
11. Bai P, Canto C, Brunyánszki A, et al. PARP-2 regulates SIRT1 expression and whole-body energy expenditure. Cell Metab. 2011; 13(4):450–460. [PubMed: 21459329]
12. Nicolás L, Martínez C, Baró C, et al. Loss of poly (ADP-ribose) polymerase-2 leads to rapid development of spontaneous T-cell lymphomas in p53-deficient mice. Oncogene. 2010; 29(19): 2877–2883. [PubMed: 20154718]
13. Yélamos J, Monreal Y, Saenz L, et al. PARP-2 deficiency affects the survival of CD4+CD8+ double-positive thymocytes. EMBO J. 2006; 25(18):4350–4360. [PubMed: 16946705]
14. Ito K, Hirao A, Arai F, et al. Regulation of oxidative stress by ATM is required for self-renewal of haematopoietic stem cells. Nature. 2004; 431(7011):997–1002. [PubMed: 15496926]
15. Nijnik A, Woodbine L, Marchetti C, et al. DNA repair is limiting for haematopoietic stem cells during ageing. Nature. 2007; 447(7145):686–690. [PubMed: 17554302]
16. Rossi DJ, Bryder D, Seita J, Nussenzweig A, Hoeijmakers J, Weissman IL. Deficiencies in DNA damage repair limit the function of haematopoietic stem cells with age. Nature. 2007; 447(7145): 725–729. [PubMed: 17554309]
17. Zhang S, Yajima H, Huynh H, et al. Congenital bone marrow failure in DNA-PKcs mutant mice associated with deficiencies in DNA repair. J Cell Biol. 2011; 193(2):295–305. [PubMed: 21482716]
18. Blanpain C, Mohrin M, Sotiropoulou PA. Passegué E. DNA-damage response in tissue-specific and cancer stem cells. Cell Stem Cell. 2011; 8(1):16–29. [PubMed: 21211780]
19. Mohrin M, Bourke E, Alexander D, et al. Hematopoietic stem cell quiescence promotes error-prone DNA repair and mutagenesis. Cell Stem Cell. 2010; 7(2):174–185. [PubMed: 20619762]
20. Orkin SH, Zon LI. Hematopoiesis: an evolving paradigm for stem cell biology. Cell. 2008; 132(4): 631–644. [PubMed: 18295580]
21. Attar EC, Scadden DT. Regulation of hematopoietic stem cell growth. Leukemia. 2004; 18(11): 1760–1768. [PubMed: 15457182]
22. Maryanovich M, Oberkovitz G, Niv H, et al. The ATM-BID pathway regulates quiescence and survival of haematopoietic stem cells. Nat Cell Biol. 2012; 14(5):535–541. [PubMed: 22446738]
23. Passegué E, Wagers AJ, Giuriato S, Anderson WC, Weissman IL. Global analysis of proliferation and cell cycle gene expression in the regulation of hematopoietic stem and progenitor cell fates. J Exp Med. 2005; 202(11):1599–1611. [PubMed: 16330818]
24. Ceccaldi R, Parmar K, Mouly E, et al. Bone marrow failure in Fanconi anemia is triggered by an exacerbated p53/p21 DNA damage response that impairs hematopoietic stem and progenitor cells. Cell Stem Cell. 2012; 11(1):36–49. [PubMed: 22683204]
25. Niedernhofer LJ. DNA repair is crucial for maintaining hematopoietic stem cell function. DNA Repair (Amst). 2008; 7(3):523–529. [PubMed: 18248857]
26. de Murcia JM, Niedergang C, Trucco C, et al. Requirement of poly(ADP-ribose) polymerase in recovery from DNA damage in mice and in cells. Proc Natl Acad Sci USA. 1997; 94(14):7303–7307. [PubMed: 9207086]

27. Villunger A, Michalak EM, Coultas L, et al. p53- and drug-induced apoptotic responses mediated by BH3-only proteins puma and noxa. Science. 2003; 302(5647):1036–1038. [PubMed: 14500851]
28. Corral J, Yélamos J, Hernández-Espinosa D, et al. Role of lipopolysaccharide and cecal ligation and puncture on blood coagulation and inflammation in sensitive and resistant mice models. Am J Pathol. 2005; 166(4):1089–1098. [PubMed: 15793289]
29. Chalmers A, Johnston P, Woodcock M, Joiner M, Marples B. PARP-1, PARP-2, and the cellular response to low doses of ionizing radiation. Int J Radiat Oncol Biol Phys. 2004; 58(2):410–419. [PubMed: 14751510]
30. Wang YV, Leblanc M, Fox N, et al. Fine-tuning p53 activity through C-terminal modification significantly contributes to HSC homeostasis and mouse radiosensitivity. Genes Dev. 2011; 25(13):1426–1438. [PubMed: 21724834]
31. Verbon EH, Post JA, Boonstra J. The influence of reactive oxygen species on cell cycle progression in mammalian cells. Gene. 2012; 511(1):1–6. [PubMed: 22981713]
32. Chen CS, Wang YC, Yang HC, et al. Histone deacetylase inhibitors sensitize prostate cancer cells to agents that produce DNA double-strand breaks by targeting Ku70 acetylation. Cancer Res. 2007; 67(11):5318–5327. [PubMed: 17545612]
33. Subramanian A, Tamayo P, Mootha VK, et al. Gene set enrichment analysis: a knowledge-based approach for interpreting genome-wide expression profiles. Proc Natl Acad Sci USA. 2005; 102(43):15545–15550. [PubMed: 16199517]
34. Na Nakorn T, Traver D, Weissman IL, Akashi K. Myeloerythroid-restricted progenitors are sufficient to confer radioprotection and provide the majority of day 8 CFU-S. J Clin Invest. 2002; 109(12):1579–1585. [PubMed: 12070305]
35. Michalak EM, Vandenberg CJ, Delbridge AR, et al. Apoptosis-promoted tumorigenesis: gamma-irradiation-induced thymic lymphomagenesis requires Puma-driven leukocyte death. Genes Dev. 2010; 24(15):1608–1613. [PubMed: 20679396]
36. Wu WS, Heinrichs S, Xu D, et al. Slug antagonizes p53-mediated apoptosis of hematopoietic progenitors by repressing puma. Cell. 2005; 123(4):641–653. [PubMed: 16286009]
37. Labi V, Erlacher M, Krumschnabel G, et al. Apoptosis of leukocytes triggered by acute DNA damage promotes lymphoma formation. Genes Dev. 2010; 24(15):1602–1607. [PubMed: 20679395]
38. Marples B. Is low-dose hyper-radiosensitivity a measure of G2-phase cell radiosensitivity? Cancer Metastasis Rev. 2004; 23(3-4):197–207. [PubMed: 15197323]
39. Saxena A, Wong LH, Kalitsis P, Earle E, Shaffer LG, Choo KH. Poly(ADP-ribose) polymerase 2 localizes to mammalian active centromeres and interacts with PARP-1, Cenpa, Cenpb and Bub3, but not Cenpc. Hum Mol Genet. 2002; 11(19):2319–2329. [PubMed: 12217960]
40. Yahata T, Takanashi T, Muguruma Y, et al. Accumulation of oxidative DNA damage restricts the self-renewal capacity of human hematopoietic stem cells. Blood. 2011; 118(11):2941–2950. [PubMed: 21734240]
41. Juntilla MM, Patil VD, Calamito M, Joshi RP, Birnbaum MJ, Koretzky GA. AKT1 and AKT2 maintain hematopoietic stem cell function by regulating reactive oxygen species. Blood. 2010; 115(20):4030–4038. [PubMed: 20354168]
42. Kim JJ, Tannock IF. Repopulation of cancer cells during therapy: an important cause of treatment failure. Nat Rev Cancer. 2005; 5(7):516–525. [PubMed: 15965493]

Europe PMC Funders Author Manuscripts

Key points

- Genetic inactivation of Parp-2 in mice, but not of Parp-1, resulted in bone marrow failure in response to sublethal γ-irradiation dose.
- Parp-2 plays an essential role in the DNA damage response in HSPC maintaining hematopoietic homeostasis under stress conditions.

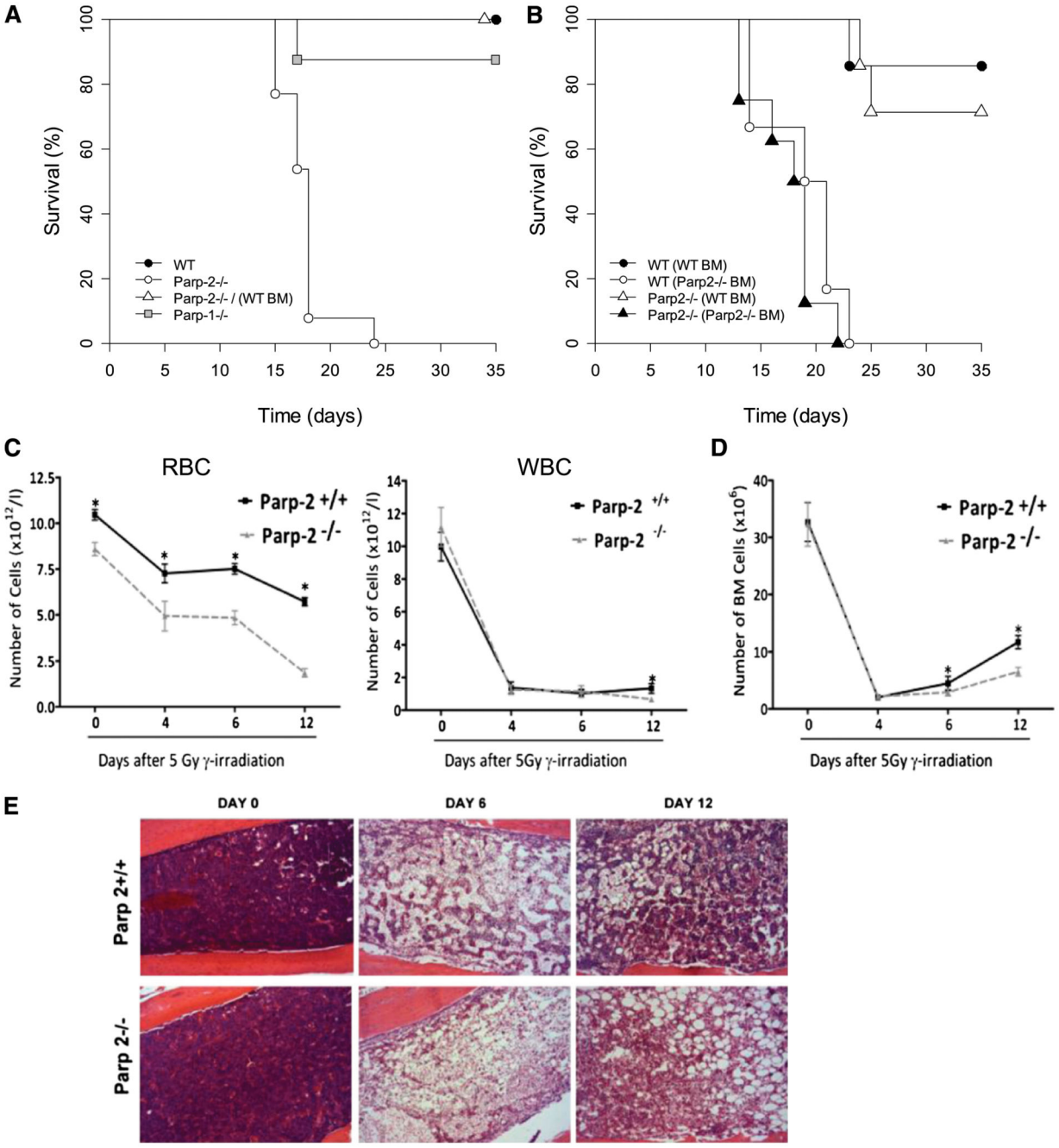

Figure 1. High sensitivity of Parp-2$^{-/-}$ mice to sublethal γ-radiation dose caused by BM failure.

(A) Kaplan-Meier survival curves, after 5 Gy of total body γ-irradiation (TBI), of 5-week-old Parp-2$^{-/-}$ (n = 13), Parp-1$^{-/-}$ (n = 8), wild-type (WT) (n = 15), and Parp-2$^{-/-}$ mice injected with 2 × 10^6 WT BM cells (Parp-2$^{-/-}$ [WT BM]; n = 5). Survival was monitored for 35 days. (B) Kaplan-Meier survival curves of reconstituted Parp-2$^{-/-}$ or WT mice after γ-irradiation. Parp-2$^{-/-}$ recipient mice were given a lethal dose of radiation (9.5 Gy) and reconstituted with 10 × 10^6 total BM cells from WT (6 recipient mice) or Parp-2$^{-/-}$ mice (6 recipient mice). Similarly, lethally irradiated WT mice were reconstituted with WT or

Europe PMC Funders Author Manuscripts

Parp-2$^{-/-}$ BM cells. After 6 weeks, these mice were given a single dose of γ-irradiation (5 Gy) and survival was monitored for 35 days. (C) Red blood cells (RBC) and white blood cells (WBC) in WT and Parp-2$^{-/-}$ mice at different time points after TBI (5 Gy). (D) Total number of BM cells (two femurs per mouse) in WT and Parp-2$^{-/-}$ mice at different time points after TBI (5 Gy). Values represent the mean ± SEM of at least 6 mice of each genotype. *Statistically significant difference ($P < .05$). (E) Hematoxylin and eosin staining of fixed femur sections from WT and Parp-2$^{-/-}$ mice before and at days 6 and 12 post irradiation (5 Gy) (original magnification × 100).

Europe PMC Funders Author Manuscripts

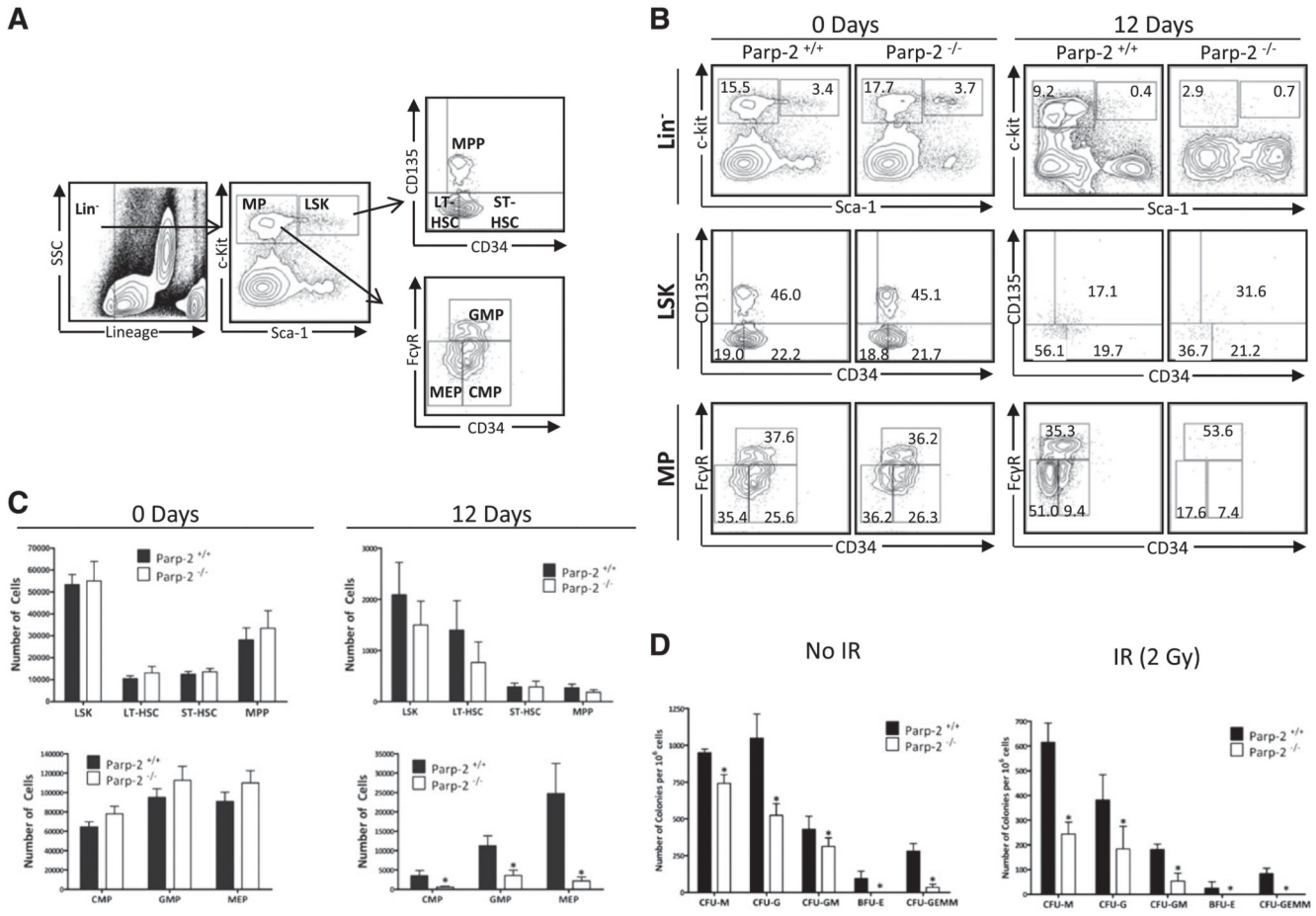

Figure 2. Parp-2 deficiency impairs the survival of HSPCs after γ-irradiation.

(A) Flow cytometry gating strategy used to analyze LSK (LT-HSC, ST-HSC, and MPP), and MP (CMP, GMP, and MEP) cells from mouse BM. (B) Representative dot-plots showing LSK (Lin^- ($CD11b^-Gr1^-B220^-CD3^-Ter119^-$) $Sca\text{-}1^+c\text{-}kit^+$), LT-HSC ($Lin^-Sca\text{-}1^+c\text{-}kit^+CD135^-CD34^-$), ST-HSC ($Lin^-Sca\text{-}1^+c\text{-}kit^+CD135^-CD34^+$), MPP ($Lin^-Sca\text{-}1^+c\text{-}kit^+CD135^+CD34^+$), CMP ($Lin^-Sca\text{-}1^-c\text{-}kit^+CD34^+Fc\gamma R^{lo}$), GMP ($Lin^-Sca\text{-}1^-c\text{-}kit^+CD34^+Fc\gamma R^{hi}$), and MEP ($Lin^-Sca\text{-}1^-c\text{-}kit^+CD34^-Fc\gamma R^{lo}$) population in Parp-$2^{-/-}$ mice and WT littermates, both in steady-state conditions and 12 days after TBI (5 Gy). Percentage of cells in the individual subpopulations with regard to each gate is indicated in each quadrant. Values represent the mean of at least 8 mice of each genotype. (C) Graph showing the absolute number of LSK, LT-HSC, ST-HSC, MPP, CMP, GMP, and MEP cells, determined using the gating strategies shown in (A). The number of cells in each population was calculated by multiplying the percentage of each population by the total number of BM cells. Values represent the mean ± SEM of at least 8 mice of each genotype. *Statistically significant difference ($P < .05$). (D) Colony-forming units in the BM of WT and Parp-$2^{-/-}$ mice. 4×10^4 BM cells from WT and Parp-$2^{-/-}$ mice, untreated (No IR) or after irradiation (IR) (2 Gy), were plated in duplicate in methylcellulose-containing media, and colonies were counted and distinguished by morphology on day 7. CFU-M, colony-forming unit-macrophage; CFU-G, colony-forming unit-granulocyte; CFU-GM, colony-forming unit-

granulocyte macrophage; BFU-E, Burst-forming unit-erythroid; CFU-GEMM, colony-forming unit-granulocyte, erythroid, macrophage, megakaryocyte. Data are presented as number of colonies per 10^6 cells. Values represent mean ± SEM from 3 independent experiments including at least 3 mice of each genotype per experiment. *Statistically significant difference ($P < .05$).

Europe PMC Funders Author Manuscripts

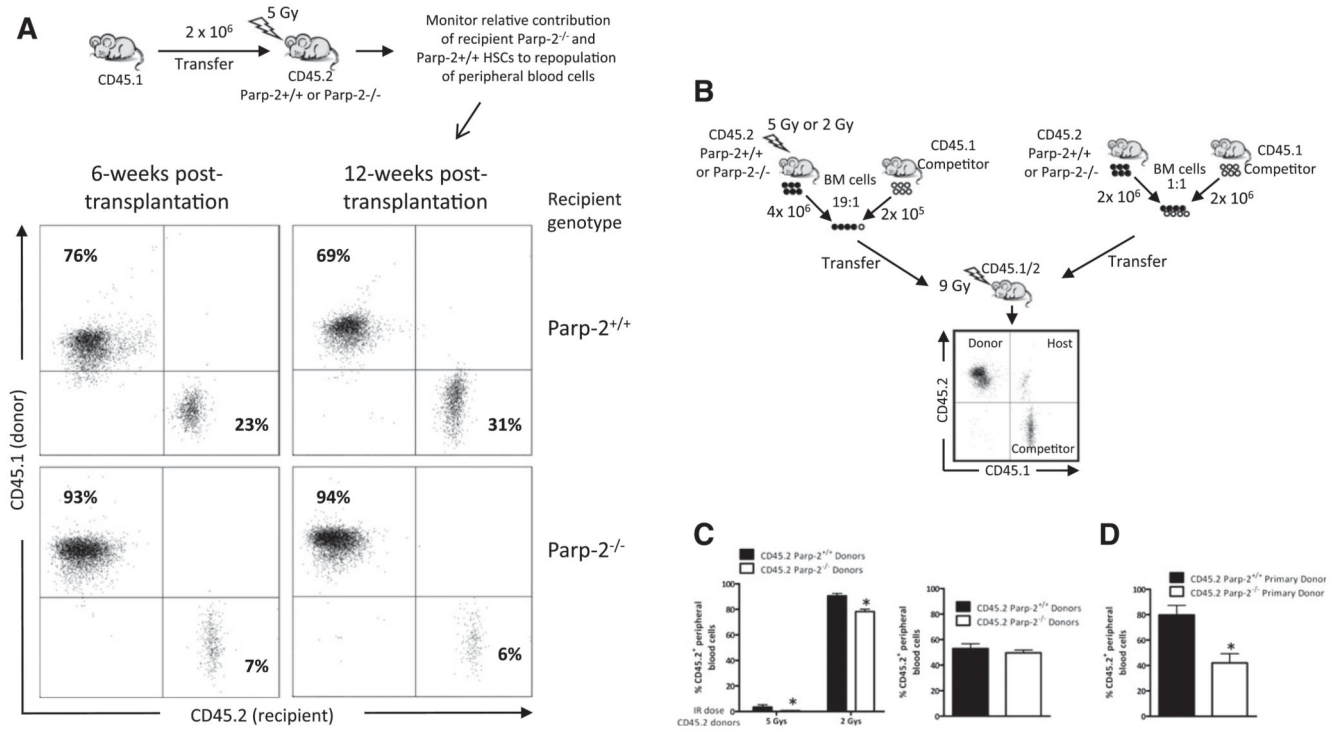

Figure 3. Parp-2 deficiency affects BM-repopulating capacity of HSCs after expansion stress.

(A) Flow cytometric analysis of peripheral blood cells isolated from either Parp-$2^{-/-}$ (n = 5) or WT (n = 5) recipient mice (CD45.2^{+}) at 6 and 12 weeks after TBI (5 Gy) and the injection of WT congenic CD45.1^{+} BM cells. Cells were stained with anti-CD45.1 and anti-CD45.2 mAb. Percentages of cells in the individual subpopulations are indicated in each quadrant. (B) Scheme detailing competitive BM reconstitution using total BM cells from irradiated (5 Gy or 2 Gy) (left) and nonirradiated (right) WT or Parp-$2^{-/-}$ donor mice expressing the CD45.2 leukocyte cell surface marker in fixed ratios with WT B6.SJL competitor BM cells expressing CD45.1 and transplanted into lethally irradiated (9 Gy) B6 x B6.SJL F1 (CD45.1/CD45.2) recipient mice. (C) Graph showing the percentage of donor-derived (CD45.2) cells in the peripheral blood of B6 × B6.SJL F1 (CD45.1/CD45.2) recipients at 12 weeks after transplantation. Values represent the mean ± SEM of at least 6 mice of each genotype. *Statistically significant difference ($P < .05$). (D) Results of secondary transplants in which each secondary recipient received 2 × 10^6 BM cells from a primary recipient 16 weeks after the primary transplantation. The graph shows the percentage of donor-derived CD45.2^{+} cells in the peripheral blood of B6 × B6.SJL F1 (CD45.1/CD45.2) recipients at 12 weeks after transplantation. Values represent the mean ± SEM of at least 6 mice of each group. *Statistically significant difference ($P < .05$).

Europe PMC Funders Author Manuscripts

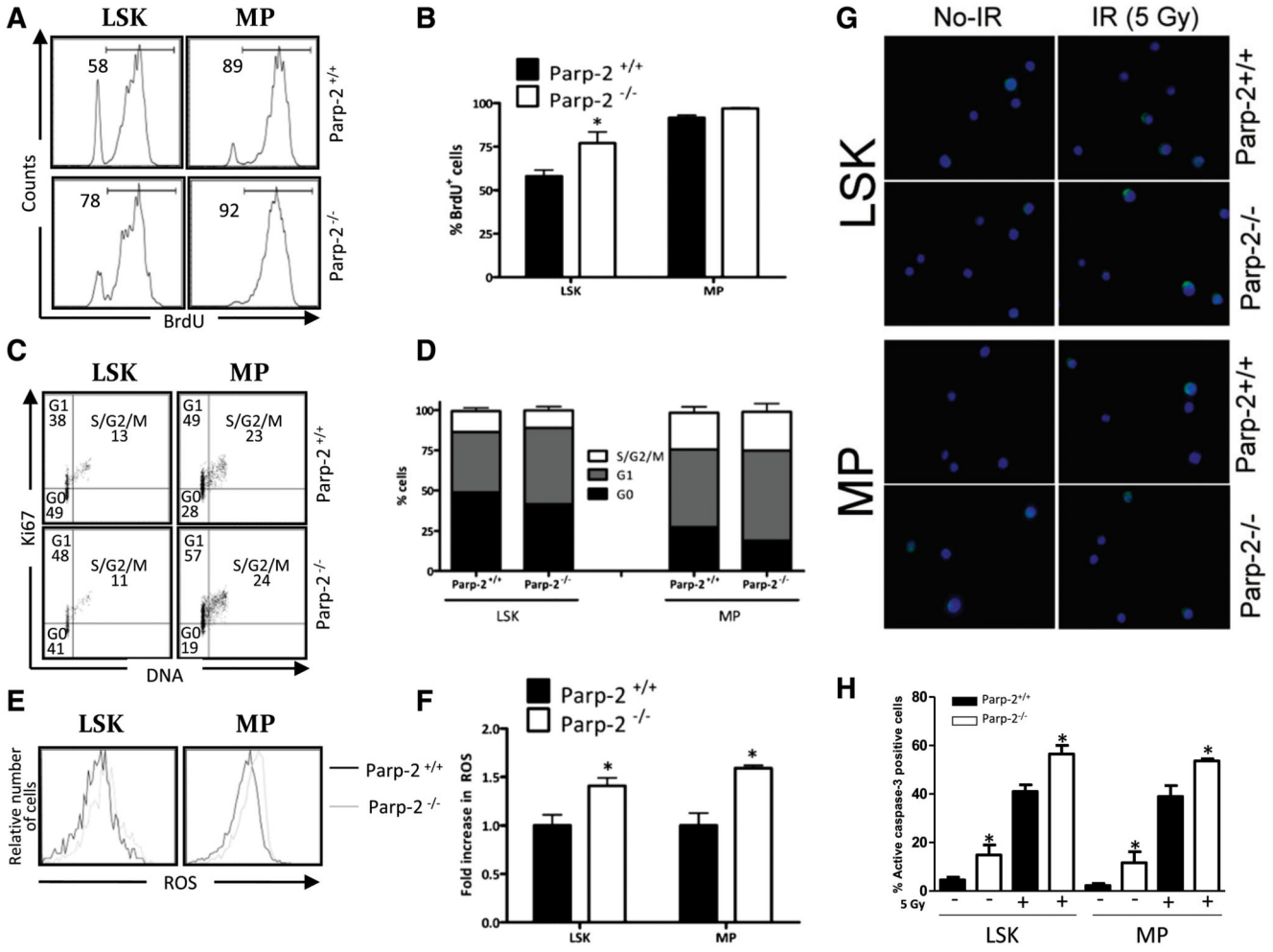

Figure 4. Effect of Parp-2 deficiency on HSPC proliferation and apoptosis.

(A-B) In vivo proliferation of Parp-$2^{+/+}$ and Parp-$2^{-/-}$ LSK and MP cells was determined by intraperitoneal injection of 6-week-old mice with BrdU (1 mg/6 g mouse weight) and provided BrdU in their drinking water for 3 days. BrdU incorporation was analyzed by flow cytometry. Representative histograms (A) from 2 independent experiments including Parp-$2^{+/+}$ (n = 3 per experiment) and Parp-$2^{-/-}$ (n = 3 per experiment) mice are shown. Numbers indicate percent proliferating ($BrdU^+$) cells. (B) Bars represent the mean ± SEM values of the percentage of $BrdU^+$ cells obtained from 6 mice per genotype. (C) Effect of Parp-2 deficiency on quiescence of LSK and MP cells. Representative staining profiles for LSK and MP cells analyzed for Ki67 and DNA content. The percentage of cells in each quadrant represents the mean from at least 6 mice in each group. (D) Percentage of Parp-$2^{+/+}$ and Parp-$2^{-/-}$ LSK and MP cells that are in G0, G1, and *S*-G2/M phases of cell cycle. Bars represent the mean ± SEM obtained from 6 mice per genotype. (E) Parp-2-deficient LSK and MP cells showed increase levels of ROS. Representative histograms showing LSK and MP cells loaded with the ROS detection reagent, 5-(and -6)-carboxy-2′,7′-difluorodihydrofluorescein diacetate (H2DFFDA). (F) The relative ROS level was calculated on the basis of the mean fluorescence intensity of the H2DFFDA and was

presented as fold induction compared with the control group. Bars represent the mean ± SEM obtained from 5 mice per genotype. (G) Representative immunofluorescence images of active caspase-3 in LSK and MP cells derived from Parp-$2^{+/+}$ and Parp-$2^{-/-}$ mice at basal and 2 hours after γ-irradiation (IR) (5 Gy). Green represents active caspase-3; blue represents DAPI. (H) Bars represent the percentage of cells positive for active caspase-3. Values represent the mean ± SEM obtained from at least 6 mice per genotype. *Statistically significant difference ($P < .05$).

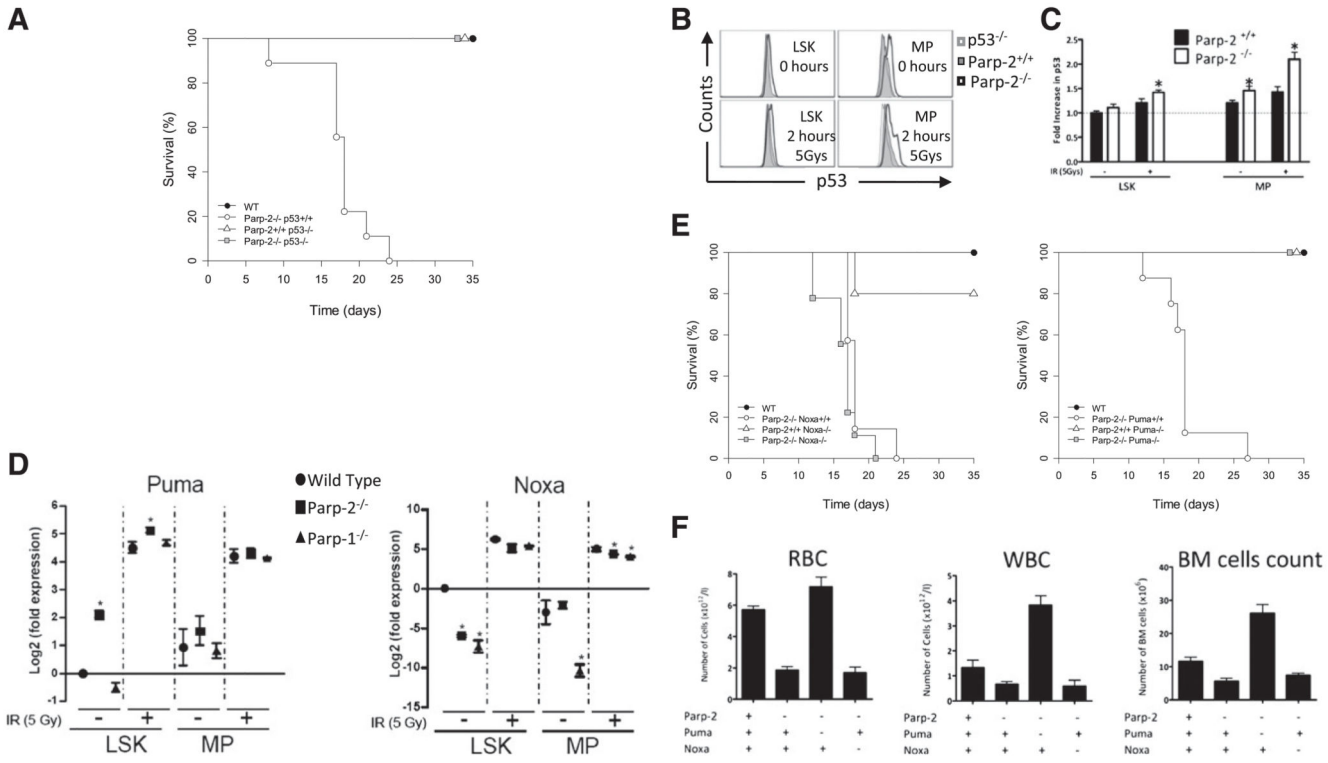

Figure 5. Effect of p53-mediated apoptotic pathways in the radiosensitivity of Parp-2 deficient mice.

(A) Kaplan-Meier survival curves for 5-week-old WT (n = 12), Parp-$2^{-/-}$$p53^{+/+}$ (n = 13), Parp-$2^{+/+}$$p53^{-/-}$ (n = 6), and Parp-$2^{-/-}$$p53^{-/-}$ (n = 5) mice after a single dose of TBI (5 Gy). (B) Representative histograms show p53 protein levels in LSK and MP cells derived from Parp-$2^{+/+}$ and Parp-$2^{-/-}$ mice at basal level and 2 hours after γ-irradiation (5 Gy). LSK and MP cells from $p53^{-/-}$ mice were included as controls. (C) The relative p53 protein levels were calculated on the basis of the mean fluorescence intensity and were presented as fold induction compared with WT cells. Bars represent the mean ± SEM obtained from 4 mice per genotype. (D) Quantitative RT-PCR analysis of Puma and Noxa mRNA expression levels in LSK and MP cells derived from WT, Parp-$2^{-/-}$, and Parp-$1^{-/-}$ mice at basal level and 2 hours after γ-irradiation (5 Gy). Samples were normalized according to p-actin expression levels. Results are expressed as log2-fold expression compared with levels measured in untreated WT LSK cells. Values represent the mean ± SEM obtained from 3 independent experiments. *Statistically significant difference ($P < .05$). (E) Kaplan-Meier survival curves for 5-week-old WT (n = 12), Parp-$2^{-/-}$$Noxa^{+/+}$ (n = 13), Parp-$2^{+/+}$ $Noxa^{-/-}$ (n = 5), Parp-$2^{-/-}$$Noxa^{-/-}$ (n = 9), Parp-$2^{-/-}$$Puma^{+/+}$ (n = 13), Parp-$2^{+/+}$$Puma^{-/-}$ (n = 6), and Parp-$2^{-/-}$$Puma^{-/-}$ (n = 9) mice after a single dose of TBI (5 Gy). Survival was monitored for 35 days. (F) Graph showing peripheral RBCs, WBCs, and total number of BM cells (2 femurs per mouse) in the different genotypes at day 12 post irradiation (5 Gy). Values represent the mean ± SEM of at least 6 mice of each genotype.

Europe PMC Funders Author Manuscripts

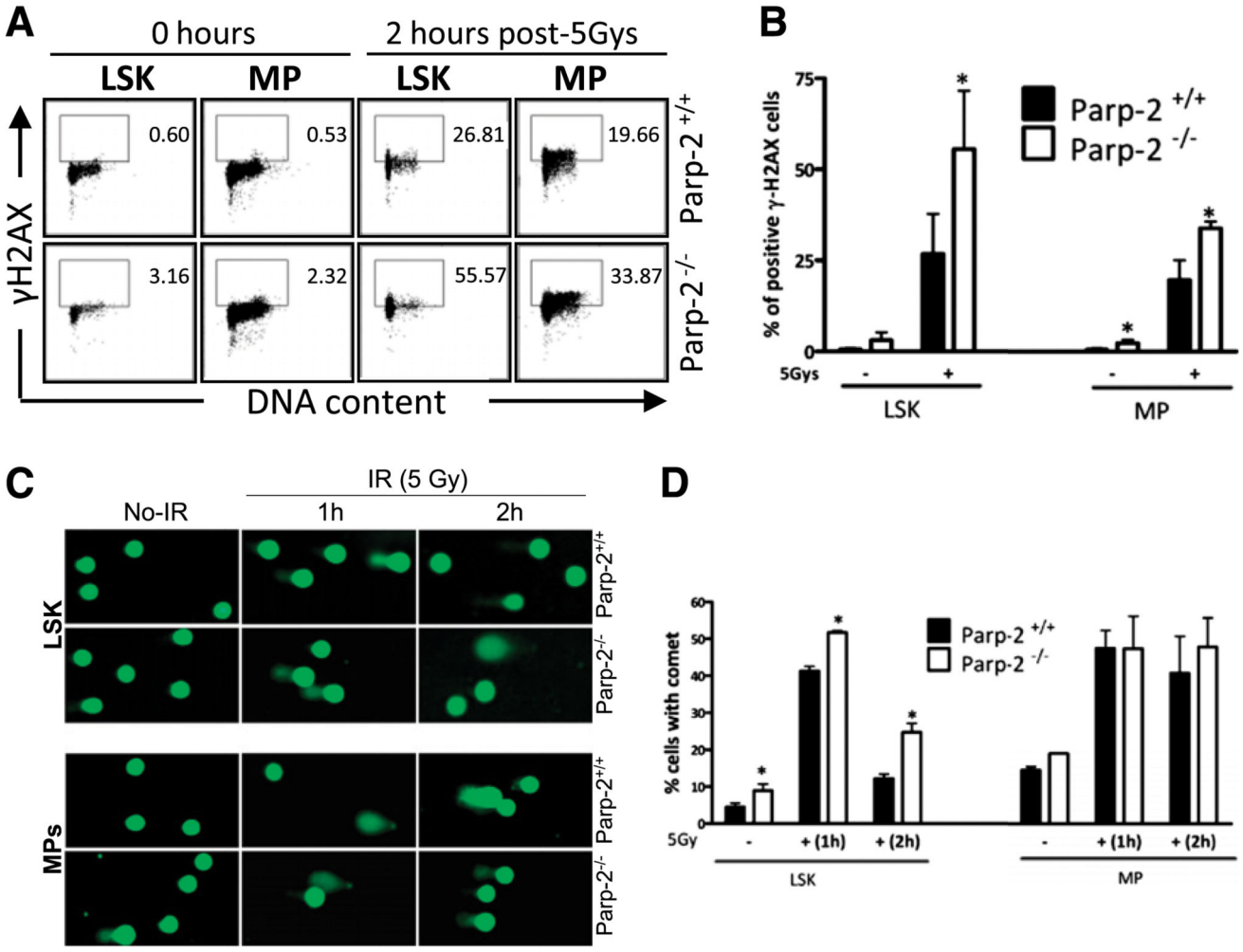

Figure 6. Accumulation of DNA damage in irradiated-Parp-2$^{-/-}$ HSPCs.

(A) Representative staining profiles of γH2AX in LSK and MP cells derived from Parp-2$^{+/+}$ and Parp-2$^{-/-}$ mice at basal level and 2 hours after γ-irradiation (5 Gy). (B) Graph showing the percentage of γH2AX-positive cells. Bars represent the mean ± SEM obtained from at least 5 mice per genotype. (C) Representative images showing DNA damage in LSK and MP cells derived from Parp-2$^{+/+}$ and Parp-2$^{-/-}$ mice at different time points after irradiation (5 Gy), visualized by alkaline comet assay. (D) Graph showing the percentage of cells with comet. An average of 100 cells was scored for each time point from each mouse. Bars represent the mean ± SEM obtained from 3 mice per genotype from independent experiments.

Europe PMC Funders Author Manuscripts

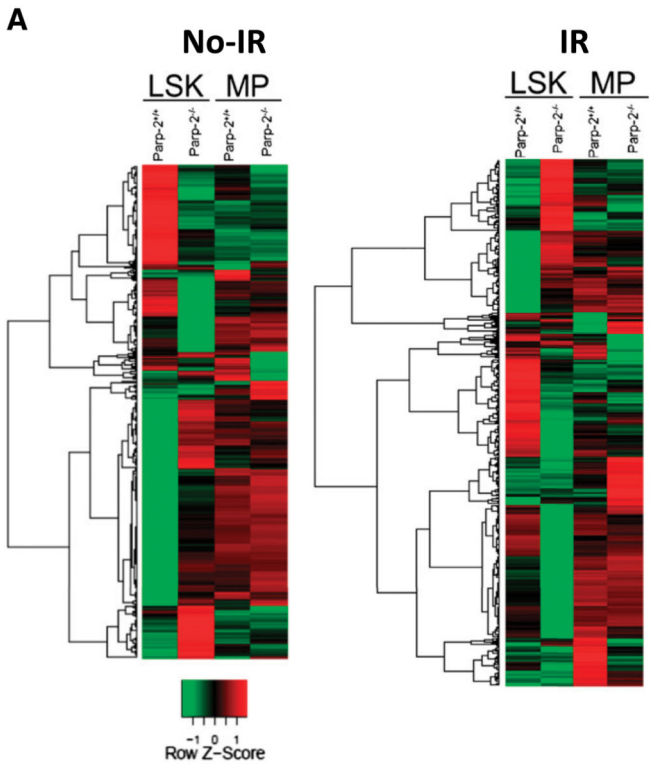

B

No-IR

Biological Process	LSK	MP
	P-value	P-value
Cell cycle mitotic	<0.00001	<0.00001
Cell cycle checkpoints	0.00383	0.00019
S phase	<0.00001	<0.00001
DNA replication	0.00122	0.00324
DNA repair	0.06471	0.00880
Activation of ATR	0.01612	0.00044
Apoptosis	n.s.	<0.00001
Apoptotic cleavage of Cell adhesion proteins	0.02063	n.s.

IR (5 Gy)

Biological Process	LSK	MP
	P-value	P-value
Cell cycle mitotic	n.s.	<0.00001
Cell cycle checkpoints	0.04750	n.s.
Base excision repair	0.00866	n.s.
Apoptosis	0.00155	<0.00001

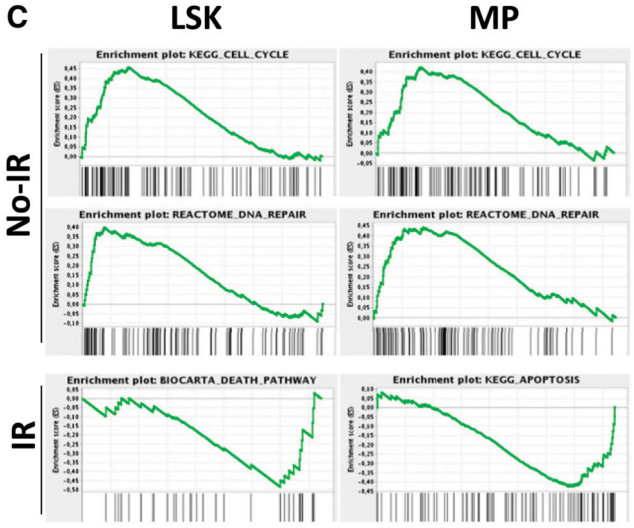

Figure 7. Gene expression profile analysis of Parp-$2^{+/+}$ and Parp-$2^{-/-}$ LSK and MP cells.

(A) Heat map representing the average normalized intensity values of all genes that are differentially expressed between WT and Parp-$2^{-/-}$ LSK and MP cells (n = 982 genes). Red indicates higher expression in Parp-$2^{-/-}$ compared with Parp-$2^{+/+}$, whereas green indicates lower expression in Parp-$2^{-/-}$ compared with Parp-$2^{+/+}$. (B) Selected differentially expressed biological processes between WT and Parp-$2^{-/-}$ LSK and MP cells. Canonical pathways gene sets were scored using the GSEA and *P* values were computed using 1000 permutations. n.s., not statistically significant. (C) Examples of GSEA plots obtained from expression microarray data. Within these plots, the green line represents the sliding enrichment score and the black bars demarcate the position of the gene set members within the ranked expression data.